# Piecewise Affine Maximum Torque per Ampere for the Wound Rotor Synchronous Machine

Bernard Steyaert
Columbia University
bernard.steyaert@columbia.edu

Ethan Swint
Tau Motors
ethan@taumotors.com

W. Wesley Pennington
Tau Motors
wesley@taumotors.com

Matthias Preindl
Columbia University
matthias.preindl@columbia.edu

***Abstract*—Power-efficient torque control of the Wound Rotor Synchronous Machine (WRSM) requires a minimization of electrical losses, namely copper and iron losses. In this paper, the Minimum Power Loss per Torque (MPLPT) optimization problem is presented and solved using a convex pareto frontier of simulated or measured data points. Magnetic saturation and cross-saturation effects are captured using sampled points throughout full-machine operation. A filtered solution set is mapped to current space using piecewise affine functions, which approximate the current using a piecewise linear function for a given torque. This set of piecewise linear functions enables a machine controller to implement MPLPT online or as an offline lookup table. Results are presented for a 65 kW, FEA-sampled WRSM.**

***Index Terms*—Loss Minimization, Motor Parameters, Piecewise Linear Techniques, Torque Control, Wound Rotor Synchronous Machine**

## I. Introduction

This research focuses on the wound rotor synchronous machine (WRSM) and minimizing electrical losses given a reference torque while taking saturation and cross-saturation into account. WRSMs are a class of electric machines used in power generation, traction (e.g., electric vehicles, EVs), and other industrial and residential applications. They have several advantages over PMSMs including: higher level of controllability due to their ability to modulate rotor flux, a large constant-power speed range, and increased cost-effectiveness given that no expensive, rare-earth magnets are required in production. Additionally, the rotor flux can be controlled to correct the power factor of the machine, which can lower the volt-amp (VA) rating on the system inverter [1]. This modulation can also be used to increase the stator current required for low speed, high torque operation, a feature advantageous for reducing cost in electric vehicles (EVs) [2]. For decades WRSMs have been used in power generation (10-300MW) [2], [3], while more recently it has proved its effectiveness in the EV space. The Renault Zoe vehicle uses WRSMs since 2012 [4]. However, WRSMs have certain drawbacks when compared to PMSMs including: higher copper losses due to the added rotor windings, and increase mechanical complexity. Finally, WRSM have a strong (nonlinear) coupling between the direct (d) and rotor (r) dimension.

Directly controlling the torque of any machine is generally difficult, as controllers are able to control and regulate some combination of voltage, current, or flux. A typical approach is to define a reference torque, which is then directly mapped to a reference set of currents. This mapping is generally not unique, and there is no optimal solution as torque is a non-convex function of current [5]. This problem is typically referred to as Maximum Torque per Ampere (MTPA), but is rephrased in this research as Minimum Power Loss per Torque (MPLPT) to include iron losses. The MPLPT problem becomes more complex with the addition of the strong saturation in magnetic flux of the WRSM, which must operate in the linear and nonlinear magnetic regimes in general to prevent high flux error during saturation and cross-saturation [6]–[14].

Existing online methods used to include a nonlinear magnetic flux into an MTPA-type optimization that can run on a microcontroller include calculating the instantaneous inductance of the machine using Extended Kalman Filters [15] and iteratively using Ferrari's method to reach a sufficiently accurate solution [16]. These methods are computationally expensive on a controller. Offline methods include adding a cross-coupling torque term and additional variables that decrease the inductance in saturation to approximate saturation effects. This method produces a ten-term cubic torque equation that is difficult to optimize [17] but can be mapped sufficiently accurate large LUT.

This research proposes using pareto-optimal simulated or experimental values to the MPLPT as candidate points for a MPLPT current path. The solution set is reduced by considering only convex pareto-optimal points, and the points are linked using a Piecewise Affine (PWA) function. This produces a set of linear functions that are computationally cheap to run on a controller for any reference torque of the machine.

This paper is organized as follows. In Section II the WRSM dynamic model is presented. In Section III the torque and power loss characteristics for the WRSM are explained, then Section IV describes the MPLPT optimization problem and solution sets. Section V describes the PWA map linking the solution sets to a continuous MPLPT path in three-dimensional current space. Section VI shows results for a simulated WRSM using FEA-simulated data, and finally Section VII concludes the

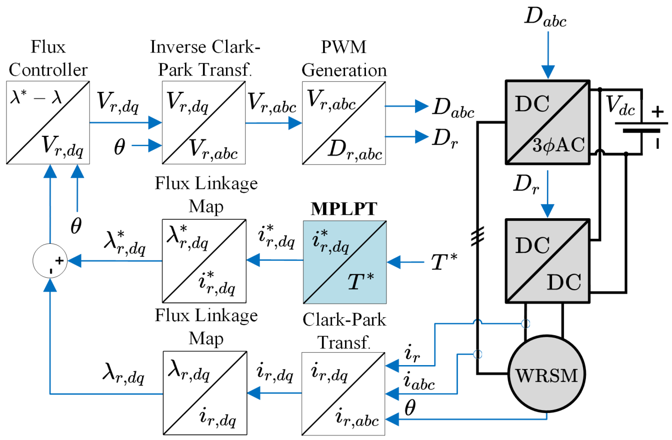

Fig. 1: WRSM motor drive (gray) with an example motor controller (white) using MPLPT function (blue) to generate reference current from reference torque

paper.

## II. WRSM Motor Model

The three-phase WRSM can be described dynamically as a state-space model [18]. For formal simplicity and the common challenges of displaying spaces higher than three, this research focuses on the most common WRSM used in motor drives: a neutral-point isolated machine (without zero-axis flux and current) and without damper windings. However, it is noted that it is trivial to generalize this research to higher dimensions. Throughout this research, we use the power-invariant Clarke transformation and the magnetic axis of the field winding is used as reference angle of the Park transformation.

The voltage equations of this WRSM are

$$\dot{\lambda}_r = v_r - R_r i_r \qquad = \bar{v}_r, \tag{1a}$$
$$\dot{\lambda}_d = \omega\lambda_q + v_d - R_s i_d \qquad = \omega\lambda_q + \bar{v}_d, \tag{1b}$$
$$\dot{\lambda}_q = -\omega\lambda_d + v_q - R_s i_q \qquad = -\omega\lambda_d + \bar{v}_q, \tag{1c}$$

where $\dot{}$ is the $\frac{d}{dt}$ operator; $\lambda_r \in \mathbb{R}$ is the rotor, i.e. field, flux linkage; $\lambda_d, \lambda_q \in \mathbb{R}$ are the d-axis and q-axis stator flux linkages respectively; $i \in \mathbb{R}$ and $v \in \mathbb{R}$ are the currents and voltages of the appropriate dimension; $R_r, R_s \in \mathbb{R}^+$ are the rotor and stator resistances, and $\omega \in \mathbb{R}$ is the synchronous speed, i.e. the electrical velocity of the machine. Furthermore, we introduce the voltages $\bar{v}$ that are the terminal voltages compensated by the winding resistive voltage drop. This concept can be generalized to include compensation for inverter nonlinear behavior such as switch on-voltage drops and dead-times [19]. The machine currents map onto machine flux with a nonlinear map $\phi : \mathbb{R}^3 \to \mathbb{R}^3$

$$\lambda_r = \phi_r(i_r, i_d, i_q), \tag{2a}$$
$$\lambda_d = \phi_d(i_r, i_d, i_q), \tag{2b}$$
$$\lambda_q = \phi_q(i_r, i_d, i_q), \tag{2c}$$

that captures magnetic coupling between axis, magnetic saturation, and cross-saturation [18]. These equations can be written as a standard state-space systems in discrete time with sampling period $T_s$

$$\lambda^+ = f(\lambda, \bar{v}), \tag{3a}$$
$$i = g(\lambda), \tag{3b}$$

where the state is the flux $\lambda = [\lambda_r, \lambda_d, \lambda_q]^T \in \Lambda$, the input is the compensated voltage $\bar{v} = [\bar{v}_r, \bar{v}_d, \bar{v}_q]^T \in \mathcal{V}$, and the measurement is the current $i = [i_r, i_d, i_q]^T \in \mathcal{I}$. The state-space variables are finite in all dimensions that are approximated with box constraints

$$\mathcal{I} = \{i \in \mathbb{R}^3 | I_{\min} \le i \le I_{\max}\}, \tag{4a}$$
$$\mathcal{V} = \{\bar{v} \in \mathbb{R}^3 | \bar{V}_{\min} \le \bar{v} \le \bar{V}_{\max}\}. \tag{4b}$$

The flux constraint is defined as a derivative of the current constraint $\Lambda = \phi \circ \mathcal{I}$. Furthermore, the flux (and current) constraints are chosen such that the rotor flux (and current) is positive $\lambda_r \ge 0$ (and $i_r \ge 0$) without loss of generality.

The dynamic equation is expressed in vector notation as [20]

$$f(\lambda, v) = (\mathbf{I} - \omega T_s \mathbf{J})\lambda + T_s \bar{v}, \tag{5}$$

where $\mathbf{J}$ is the 90° rotation matrix in the dq plane

$$\mathbf{J} = \begin{bmatrix} 0 & 0 & 0 \\ 0 & 0 & -1 \\ 0 & 1 & 0 \end{bmatrix}. \tag{6}$$

The output function $g : \mathbb{R}^3 \to \mathbb{R}^3$ is the inverse of the nonlinear flux map $\phi(\cdot) = [\phi_r(\cdot), \phi_d(\cdot), \phi_q(\cdot)]^T$. Typically, $\phi(\cdot)$ is bijective and the output function is defined as

$$g(\lambda) = \phi^{-1}(\lambda) \tag{7}$$

The map $\phi(\cdot)$ is typically obtained with with finite element analysis (FEA) or obtained with experimental measurement campaigns. The equation for relating current to flux linkage in the WRSM without saturation has the form

$$\lambda = \mathbf{L}i + \psi, \tag{8}$$

where $\mathbf{L} \in \mathbb{R}^+_{3\times3}$ is the inductance matrix and $\psi \in \mathbb{R}_{3\times1}$ is the flux-offset vector

$$\mathbf{L} = \begin{bmatrix} L_{rr} & L_{rd} & L_{rq} \\ L_{dr} & L_{dd} & L_{dq} \\ L_{qr} & L_{qd} & L_{qq} \end{bmatrix}, \quad \psi = \begin{bmatrix} \psi_r \\ \psi_d \\ \psi_q \end{bmatrix}. \tag{9}$$

The diagonal terms of $\mathbf{L}$ are the self-inductances of the rotor ($L_{rr}$) and stator ($L_{dd}$, $L_{qq}$), while the non-diagonal terms are the mutual inductances between the three axis. Typically $L_{rq}$, $L_{dq}$, $L_{qr}$, and $L_{qd}$ are negligible. In this formulation $\mathbf{L}$ is constant and the fluxes are linearized as shown in Figure 2.

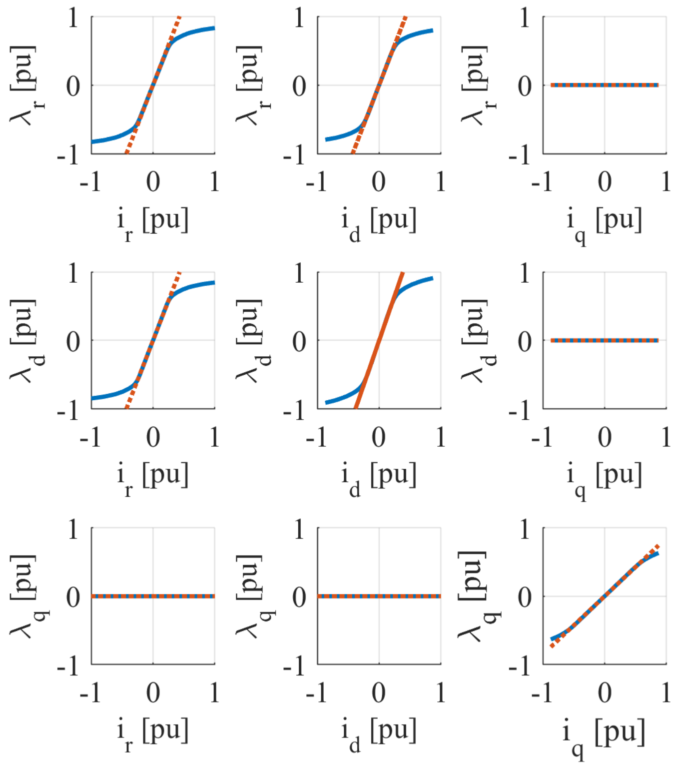


Fig. 2: WRSM flux vs current: experimental (blue), example linearization through origin (orange)

### III. Motor Torque and Power Loss Models

In many machine applications, the input to the control system is a desired or reference torque $T^*$ [Nm], while the controller is able to directly actuate winding rotor and stator voltages $\bar{v}$ and thus currents $i$. Thus it is desirable to create a direct mapping between torque and current in a way that minimizes electrical losses in the machine. For the WRSM an example control diagram is shown in Figure 1.

The machine torque per pole pair is

$$\tau_p(i,\lambda) = \tau(i,\lambda)/p = i^T \mathbf{J}\lambda, \tag{10}$$

where $\tau : \mathbb{R}^6 \to \mathbb{R}$ is the machine torque and $p$ is the number of pole pairs.

Expanding $\lambda$ using equation 8 yields the quadratic equation

$$\tau_p(i) \approx i^T \mathbf{J}\mathbf{L}i + i^T \mathbf{J}\psi, \tag{11}$$

a linearized approximation of $\tau_p(i)$ using $\phi(\cdot)$. $\tau_p(i) = T^*$ can be shown to be a saddle point of $\tau_p(i)$, as the Hessian matrix $\mathbf{H}(\tau_p(i) = T^*)$ has positive and negative eigenvalues.

The proposed MPLPT concept can be combined with any power loss models. The simplest has quadratic terms for winding losses $\pi_{lw} : \mathbb{R}^6 \to \mathbb{R}$ and core losses $\pi_{lc} : \mathbb{R}^6 \to \mathbb{R}$ of an electric motor [21]. The combined power loss is $\pi_l : \mathbb{R}^6 \to \mathbb{R}$

$$\pi_l(i,\lambda) = \pi_{lw}(i,\lambda) + \pi_{lc}(i,\lambda). \tag{12}$$

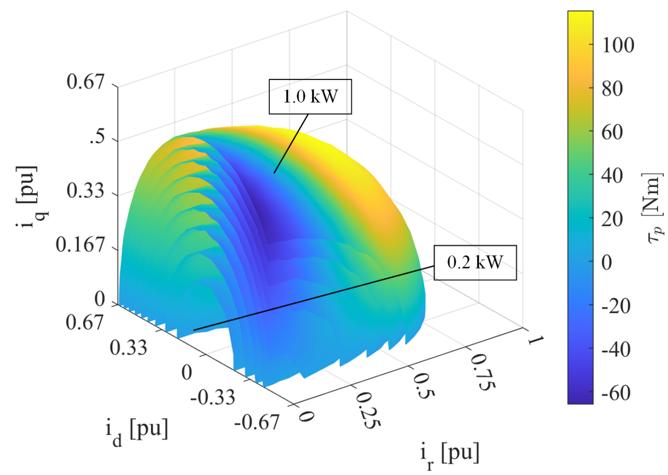


Fig. 3: $P_l = \pi_l(i,\lambda)$ for $P_l = \{0.2$ kW, 0.3 kW, 0.4 kW, 0.5 kW, 0.6 kW, 0.7 kW, 0.8 kW, 0.9 kW, 1.0 kW$\}$

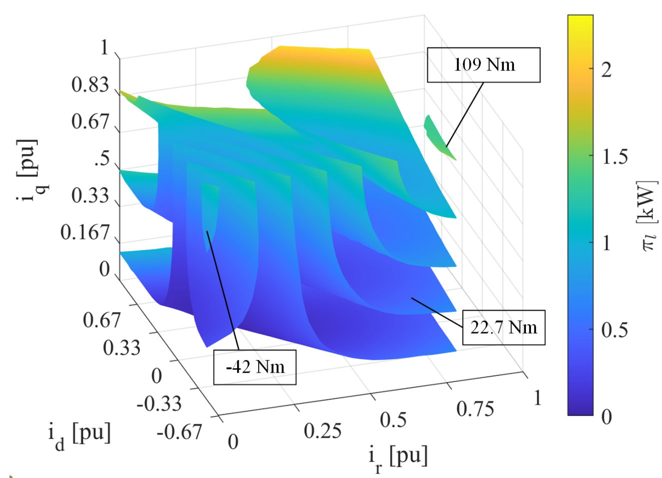


Fig. 4: $T_p = \tau_p(i,\lambda)$ for $T_p = \{-42$ Nm/p, $-20.4$ Nm/p, 1.1 Nm/p, 22.7 Nm/p, 44.3 Nm/p, 65.9 Nm/p, 87.4 Nm/p, 109 Nm/p$\}$

These losses are approximated by $\phi(\cdot)$ and are defined over the sets (20) and (19)

$$\pi_{lw}(i,\lambda) \approx i^T \mathbf{R} i, \tag{13a}$$
$$\pi_{lc}(i,\lambda) \approx \omega^2 \lambda^T \mathbf{G}\lambda, \tag{13b}$$

where the matrix $\mathbf{R}$ defines the winding resistances that approximates DC and (skin effect and proximity effect) AC winding losses [22], [23]. The matrix $\mathbf{G}$ defines the core conductance that approximates (eddy current and hysteresis effect) core losses and can be interpreted as a local approximation of the Steinmetz equation [21].

Iso-power-loss and iso-torque surfaces are shown in Figures 3 and 4 respectively.

## IV. Minimum Power Loss per Torque

### A. Problem Statement

The MPLPT targets minimizing losses (equations 13a and 13b) for a given reference torque $T^*$. The output is a reference current $i^*$ and reference flux $\lambda^*$. The most general form of the problem is stated as follows: for a torque reference $T^*$, the MPLPT current and flux references are

$$[i^*, \lambda^*] = \underset{i \in \mathcal{I}, \lambda \in \Lambda, \bar{v} \in \mathcal{V}}{\arg\min} \quad \pi_l(i, \lambda), \tag{14a}$$

$$\text{subj. to} \quad f(\lambda, \bar{v}) = \lambda, \tag{14b}$$

$$g(\lambda) = i, \tag{14c}$$

$$\tau_p(i, \lambda) = T_p^*. \tag{14d}$$

The objective function 14a being minimized is electrical losses from equation 12. Constraint 14b is the flux $\lambda$ and voltage $\bar{v}$ relationship from equation 1 and requires steady state operating points ($\dot{\lambda} = 0$). Constraint 14c links current to flux using $\phi(\cdot)$, and 14d constrains the quadratic torque function to the specific reference torque of interest $T_p^*$.

The solution set for all $T_p^* \in \mathcal{T}$, where $\mathcal{T}$ is the set of allowable machine torques, will be sets of currents $\underline{\mathcal{I}}$, fluxes $\underline{\Lambda}$, torques $\underline{\mathcal{T}}$, and power losses $\underline{\mathcal{P}}$ where

$$\underline{\mathcal{I}} = \{i^* \in \mathcal{I}, \text{s.t. Eqn. } 14\} \in \mathbb{R}^3 \tag{15a}$$

$$\underline{\Lambda} = \{\lambda^* \in \Lambda, \text{s.t. Eqn. } 14\} \in \mathbb{R}^3 \tag{15b}$$

$$\underline{\mathcal{T}} = \{T^* \in \mathcal{T}, \text{s.t. Eqn. } 14\} \in \mathbb{R} \tag{15c}$$

$$\underline{\mathcal{P}} = \{P_l^* \in \mathcal{P}, \text{s.t. Eqn. } 14\} \in \mathbb{R}. \tag{15d}$$

which we can combine as

$$\underline{\Gamma} = \{\underline{\mathcal{T}}, \underline{\mathcal{P}}, \underline{\mathcal{I}}, \underline{\Lambda}\} \in \mathbb{R}^8. \tag{16}$$

This optimization problem NP-Hard to solve due to the functions $\pi_l(i, \lambda)$, $\tau_p(i, \lambda)$, and state space model equations $f(\lambda, v)$ and $g(\lambda)$, thus there is no analytical solution for $\underline{\Gamma}$. An example solution for one specific $T_p \in \underline{\mathcal{T}}$ is shown in Figure 5 showing torque and powerloss surfaces.

### B. Quantitative Solution to MPLPT

This research focuses on solving the MPLPT problem assuming low speed operation. In these conditions, the copper loss is dominant, i.e. $\pi_{lw}(\cdot) \gg \pi_{lc}(\cdot)$, and the machine operates below base speed $\omega < \omega_b$, i.e. no field weakening.

Taking a large sample of random experimental or simulated datapoints can yield an approximate solution to equation 14. FEA-simulated data points will have a current $i$ and flux $\lambda$, while experimental data points will only have a known current $i$ and an approximated flux $\lambda$ using flux-linkage map approximations via $\phi$. These points can be directly mapped to a torque per pole pair $T_p$ and powerloss $P_l$ using $\tau_p(i, \lambda)$ and $p_l(i, \lambda)$.

The set of all experimental datapoints is denoted

$$\Gamma = \{\mathcal{T}, \mathcal{P}, \mathcal{I}, \Lambda\} \in \mathbb{R}^8 \tag{17}$$

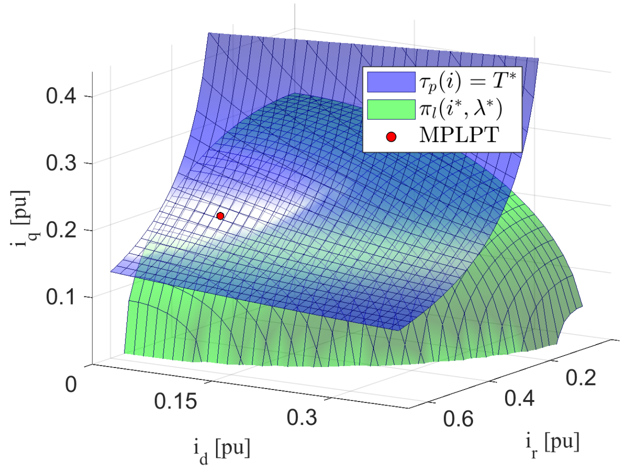


Fig. 5: Solution to MPLPT showing $\tau_p(i) = T^*$ (blue), minimized $\pi_l(i^*, \lambda^*)$ (green), and solution point (red).

where a single point $\Gamma_j$ has four components. The value of each component for each point can be denoted $\Gamma_{j,k}$ where $j$ is the component and $k$ is the index of the value. For example $\Gamma_{1,1}$ is the torque of the first data point. The set of just one component, say torque, for all points can be denoted $\Gamma_{1,k}$, while the collection of all components for one value, say the first value, can be denoted $\Gamma_{j,1}$.

The datapoints can be plotted according to their power loss, $\Gamma_{2,k}$, and inverse torque, $\Gamma_{1,k}^{-1}$, against $\underline{\Gamma}$ to see which points are the most optimal.

From the set of all datapoints $\Gamma$, there will be pareto-optimal, or efficient, values. In this case pareto-optimal value is defined as a value in $\Gamma$ that cannot further decrease $\Gamma_{1,k}^{-1}$ without increasing $\Gamma_{2,k}$ or vice-versa [24].

The set of all pareto-optimal points is called a pareto frontier. The pareto frontier for a WRSM can be denoted $\Gamma_p$. The points in the pareto frontier will all have unique torques.

The pareto frontier points $\Gamma_p$ produced by this method can be considered candidate points for a general MPLPT function that will exist in three-dimensional current space $\mathcal{I}$.

It can be noted that a line connecting all pareto-optimal points is not necessarily convex. A new set $\Gamma_c$ is defined as the largest subset of pareto-optimal points that creates a convex, piecewise linear function when line segments are added between the points.

The point $\Gamma_{j,x}$ that corresponds to minimum torque $T_{p,\min} \in \mathcal{T}_p$ will always be in $\Gamma_c$ because the minimum torque point occurs at zero losses, and no point can have negative losses. Furthermore the point $\Gamma_{j,x}$ corresponding to maximum torque $T_{p,\max} \in \mathcal{T}_p$ will also always be in this set as no point can have higher torque, regardless of losses. By definition $\Gamma \subseteq \Gamma_p \subseteq \Gamma_c$.

Because points in $\underline{\Gamma}$ are MPLPT optimal and $\Gamma_c$ are not, the losses for a point in $\Gamma_c$ will always be greater than or equal to the losses in $\underline{\Gamma}$ with the same torque. So $\Gamma_c$

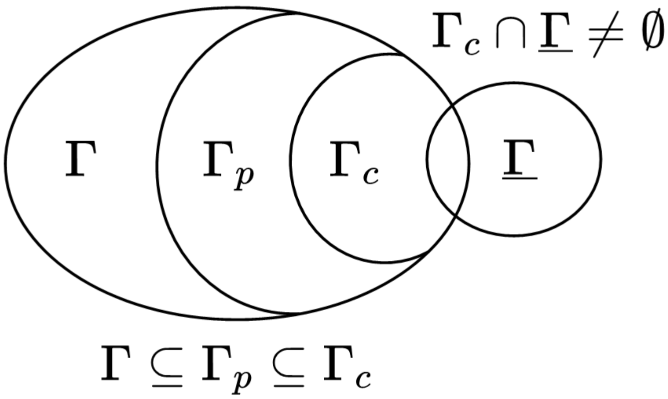


Fig. 6: Diagram showing relationship between the sets $\Gamma, \Gamma_p, \Gamma_c$, and $\underline{\Gamma}$

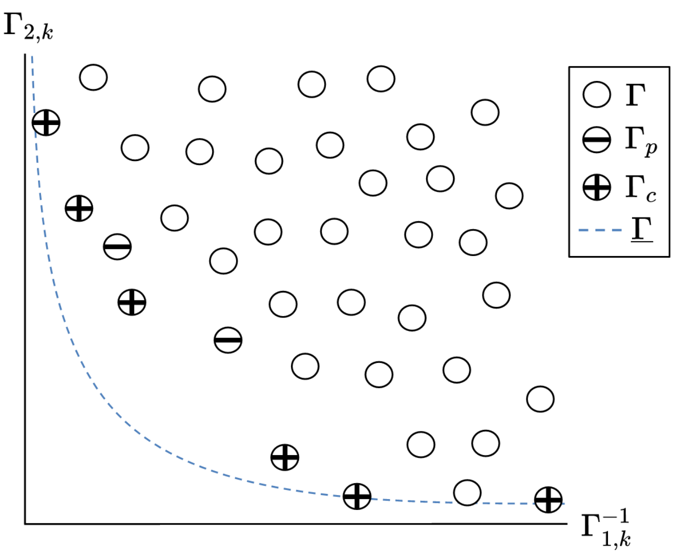


Fig. 7: Example points of $\Gamma, \Gamma_p, \Gamma_c$, and $\underline{\Gamma}$ shown on power loss $\Gamma_{2,k}$, and inverse torque $\Gamma_{1,k}^{-1}$ axis

may contain points in $\underline{\Gamma}$, or $\Gamma_c \cap \underline{\Gamma} \neq \emptyset$. The relationships between the sets $\Gamma, \Gamma_p, \Gamma_c$, and $\underline{\Gamma}$ is shown in Figure 6, and example points of the sets are shown in Figure 7.

Connecting convex pareto-optimal points $\Gamma_c$ with line segments produces values that are more optimal than using any interior pareto-optimal points. Connecting pareto-optimal points using straight line segments is an approximation that is only valid for densely-sampled points. Adjacent points in $\Gamma_c$ must be within a minimum $\epsilon$ euclidean distance of each other to be considered close enough to approximate a line between them. If two points are not close enough to meet this requirement, more points must be simulated or measured. Specifying what this distance is is outside the scope of this paper.

Generating a convex pareto frontier can be obtained using a modified divide and conquer algorithm for a set of solutions [25]. Linking the convex pareto frontier line segments from two-dimensional ($\Gamma_{1,k}^{-1}, \Gamma_{2,k} \in \mathbb{R}^2$) space to three-dimensional ($\Gamma_{3,k} \in \mathbb{R}^3$) current space can be

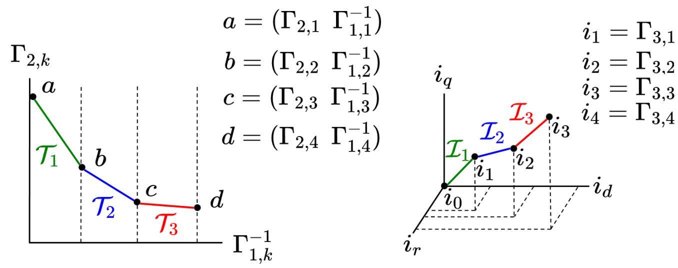


Fig. 8: (Left) Using four experimental data points ($\Gamma_{j,1}$, $\Gamma_{j,2}$, $\Gamma_{j,3}$, $\Gamma_{j,4}$) to partition torque-powerloss space into three two-dimensional simplices ($\mathcal{T}_1$, $\mathcal{T}_2$, $\mathcal{T}_3$) and the corresponding three, one-dimensional simplices in current space ($\mathcal{I}_1$, $\mathcal{I}_2$, $\mathcal{I}_3$)

modelled using a piecewise affine map.

## V. Piecewise Affine Map for MPLPT

This research proposes to express the approximate MPLPT solution path as piecewise-affine (PWA) function. PWA maps divide a nonlinear map into $M$ domains over which the function is linearized [26]. The torque domain $\Gamma_{1,k}$ is partitioned into torque regions $\mathcal{T}_j$, but can equivalently be partitioned into powerloss regions. Moving forward points in this space are interchangeably described as torques $T_{p,k}$ or $\Gamma_{1,k}$ values equivalently. Similarly the current domain $\Gamma_{3,k}$ will be partitioned into current regions $\mathcal{I}_j$, and currents can be described by $i_k$ or $\Gamma_{3,k}$.

Hence we express the PWA torque to current map, or MPLPT function, $h(T_p)$ as

$$i = h(T_p) \approx h_{PWA}(T_p) = \begin{cases} m_1 T_p + i_1, & T_p \in \mathcal{T}_1, \\ m_2 T_p + i_2, & T_p \in \mathcal{T}_2, \\ \quad \cdots & \\ m_M T_p + i_M, & T_p \in \mathcal{T}_M, \end{cases} \tag{18}$$

where $i = m_j T_p + i_j$ is the affine equation that maps torques-powerloss points $T \in \mathcal{T}_j$ onto current points $i \in \mathcal{I}_j$ and $\mathcal{I}_j$ is the image of the domain $\mathcal{T}_j$. The torque simplices must cover the full range of machine torques, or $\{\mathcal{T}_1 \cup \mathcal{T}_2, \dots \mathcal{T}_M = \mathcal{T}$. The affine map is defined by the three-dimensional current slope and a current offset. This is seen on the left plot of Figure 8. The points used to create $h(T)$ are the set $\Gamma_c$ defined in Section IV and the process of using the points to create $h(T)$ is described next.

PWA maps divide the original domain into $M$ sets. Each subset is defined to be a simplex, which is the simplest possible polytope in any $D$-dimensional space and a line segment in the single dimension of the given problem. A $D$-dimensional simplex can be defined as the convex hull of its $D+1$ vertices (called the V-notation; alternatively, a simplex can be defined by its by its faces defined as affine inequalities called the H-notation [27])

$$\mathcal{T}_j = \mathcal{H}(\{T_{j_0}, T_{j_1}\}), \tag{19}$$

where $T_{j_0}, T_{j_1} \in \mathcal{T}$. Each torque simplex $\mathcal{T}_j$ forms a domain of an affine map that maps into the current simplex

$$\mathcal{I}_j = \mathcal{H}(\{i_{j_0}, i_{j_1}\}), \tag{20}$$

where $i_{j_0}, i_{j_1} \in \mathcal{I}$. The general position of the defining set of measurement points (convex) implies that the vertices of each simplex are linearly independent and full dimension (not degenerate). Example simplices that are linked in both spaces are shown in figure 8.

Each line segment $\mathcal{T}_j$ is defined by two vertices. Let one vertex $T_{j_0}$ be the support vector such that we can move the origin $\bar{T} = T - T_{j_0}$. In the shifted dimension, the simplex is defined by

$$\bar{\mathcal{T}_j} = \mathcal{H}(\{0, \bar{T}_{j_1}\}), \tag{21}$$

where $\bar{T_{j_1}} = T_{j_1} - T_{j_0}$ where $\bar{T_{j_1}}$ spans the simplex. Furthermore, we shift the current space in the same way, $\bar{i} = i - i_{j_0}$ that results in the simplex

$$\bar{\mathcal{I}_j} = \mathcal{H}(\{0, \bar{i}_{j_1}\}), \tag{22}$$

where $\bar{i}_{j_1} = i_{j_1} - i_{j_0}$ and $\bar{i_{j_1}}$ spans the simplex. The $D = 1$ simplices and the shift of origin are illustrated in Figure 9.

The nonzero vertices can be interpreted as a basis and since an affine map is an isomorphism, the relative position of a vector in the current and flux simplex is the same

$$\bar{T} = a\bar{T}_{j_1}. \tag{23}$$

The $a$ coefficient can be obtained similar to how space vector modulation (SVM) computes relative on-times [26].

We project $\bar{T}$ onto the basis of $\bar{\mathcal{T}_j}$

$$p_j = \text{proj}_{\bar{T}_{j_1}} \bar{T} = \frac{\bar{T}_{j_1} \cdot \bar{T}}{\|\bar{T}_{j_1}\|}, \tag{24}$$

and obtain the relative length of the vector by dividing the magnitude of the projection with the magnitude of the basis vector

$$a = \frac{\|p_j\|}{\|\bar{T}_{j_1}\|}. \tag{25}$$

To find the current vector $\bar{i}$, we multiply $a$ with the basis vector of $\bar{i}_j$, $\bar{i_{j_1}}$

$$\bar{i} = a\bar{i}_{j_1}. \tag{26}$$

Setting the $a$ coefficients in equations 23 and 26 equal

$$\frac{\bar{T}}{\bar{T}_{j_1}} = \frac{\bar{i}}{\bar{i}_{j_1}} \tag{27a}$$

and solving for $i$ yields the resulting linear map

$$i = m_j T + i_j \tag{27b}$$

where $m_j = \frac{i - i_{j_0}}{T_{j_1} - T_{j_0}}$ and $i_j = i_{j_0} - m_j T_{j_0}$ A visualization of this is shown in Figure 9.

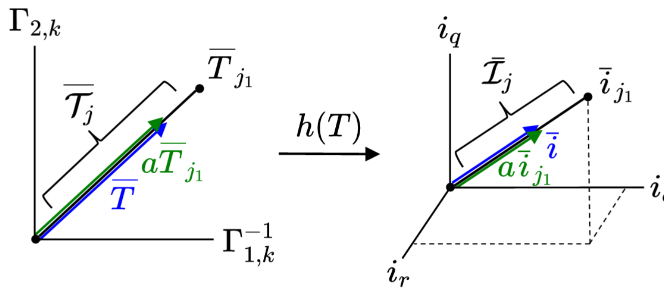


Fig. 9: Torque-powerloss shifted simplex $\overline{\mathcal{T}}_j$ and projected vector $\overline{T}_{j_1}$ mapped to shifted current simplex $\bar{\mathcal{I}}_j$ and projected vector $\bar{i}$ by PWA function $h(T)$

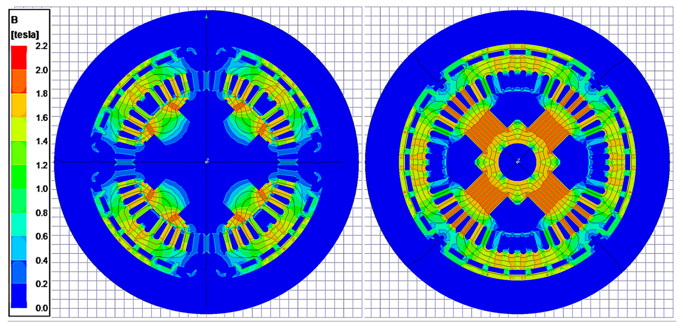


Fig. 10: WRSM cross section showing a saturated flux density $B$ distribution in Tesla at $i_q = 1$[pu] (left), and $i_d = 1$[pu] (right)

## VI. Results

A typical path of interest in machine control is the MPLPT path from the most negative machine torque to the most positive. A 65 kW WRSM with the parameters listed in Table I is used to validate the MPLPT formulation and solutions. Figure 10 shows a cross section of the machine.

TABLE I: WRSM Motor Drive Parameters

| Parameter | Value |
|---|---|
| Turns ratio $N_f/N_s$ | 39 |
| Pole pairs | 2 |
| Stator resistance | 11.732 mΩ |
| Rotor resistance (stator referred) | 5.461 mΩ |
| Shaft inertia | 22.76E-3 kg m$^2$ |
| Switching frequency | 10 kHz |
| Sampling frequency | 20 kHz |
| Nameplate r-axis inductance $L_r$ | 1.956 mH |
| Nameplate d-axis inductance $L_d$ | 2.420 mH |
| Nameplate q-axis inductance $L_q$ | 0.789 mH |
| DC-link voltage | 325 V |
| Maximum power | 65 kW |
| Maximum torque | 220 Nm |

In this case the motor has a torque range of 0 Nm/p to 112 Nm/p and copper loss range from 0 kW to 3.23 kW. Figure 11 shows the set of points $\Gamma$ and pareto frontier $\Gamma_p$ collected using FEA-simulated data for the WRSM. It is clear from this example that there are too many pareto-optimal points $\Gamma_p$ to all be used in a MPLPT path.

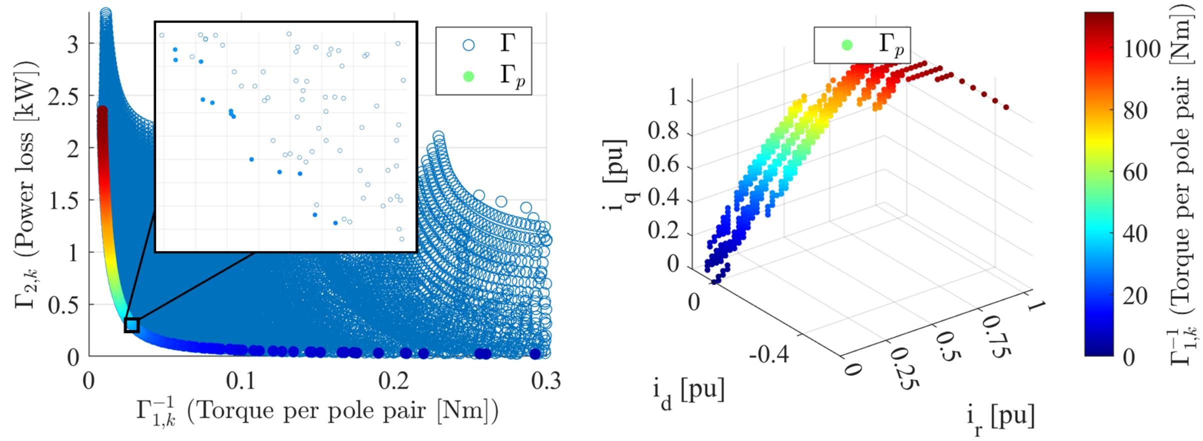


Fig. 11: Experimental results: (Left) All simulated points $\Gamma$ and pareto-optimal solutions $\Gamma_p$, (Right) corresponding three-dimensional MPLPT currents that will be candidate points for MPLPT

The resulting pareto-convex points $\Gamma_c$ are shown in Figure 12. Applying the PWA map $h(T)$ to the set of pareto-convex points yields the piecewise linear function shown in Figure 13. The function $h(T)$ in this case follows an occasionally jagged but mostly smooth curve. The distance between the points varies. There are 60 points in $\Gamma_c$ and 59 line segments that create the PWA map.

Further filtering of points in $\Gamma_c$ or a different way to filter out points in $\Gamma$ to produce a different $h(T)$ can be implemented to obtain certain qualities in the MPLPT path that can include: convexity, smoothness, and more. Costs can be assigned to the distance between points, angle of adjacent line segments, and other parameters. These considerations are currently an active area of research. The chosen method in this study strictly minimized power losses for torque without consideration for other potentially desirable qualities of the MPLPT path.

## VII. Conclusion

In this study, the Minimum Power Loss per Torque (MPLPT) problem was presented, and a novel numerical solution is was proposed. The solution set was reduced using convex pareto-optimal points, which were linked together in three-dimensional current space using Piecewise Affine (PWA) functions to create a continuous current path for all machine torques. The result was validated using simulated FEA data and shows promising results. Further research can be conducted to refine the MPLPT path to give it qualities such as smoothness and convexity.

## References


[1] A. Dòria-Cerezo, C. Batlle, and G. Espinosa-Pérez, "Passivity-based control of a wound-rotor synchronous motor," *IET Control Theory & Appl.*, vol. 4, pp. 2049–2057, 2010.

[2] C. Rossi, D. Casadei, A. Pilati, and M. Marano, "Wound Rotor Salient Pole Synchronous Machine Drive for Electric Traction," in *Conf. Rec. IEEE Ind. Appl. Conf., IAS Annu. Meet.*, vol. 3, pp. 1235–1241, Oct. 2006, iSSN: 0197-2618.

[3] A. Doria-Cerezo, V. I. Utkin, R. S. Munoz-Aguilar, and E. Fossas, "Control of a Stand-Alone Wound Rotor Synchronous Generator: Two Sliding Mode Approaches via Regulation of the d-Voltage Component," *IEEE Trans. Control Syst. Technol.*, vol. 20, no. 3, pp. 779–786, May. 2012.

[4] J. de Santiago, H. Bernhoff, B. Ekergard, S. Eriksson, S. Ferhatovic, R. Waters, and M. Leijon, "Electrical Motor Drivelines in Commercial All-Electric Vehicles: A Review," *IEEE Trans. Veh. Technol.*, vol. 61, no. 2, pp. 475–484, Feb. 2012.

[5] Y. Miao, H. Ge, M. Preindl, J. Ye, B. Cheng, and A. Emadi, "Mtpa fitting and torque estimation technique based on a new flux-linkage model for interior-permanent-magnet synchronous machines," *IEEE Transactions on Industry Applications*, vol. 53, DOI 10.1109/TIA.2017.2726980, no. 6, pp. 5451–5460, 2017.

[6] N. Bedetti, S. Calligaro, and R. Petrella, "Stand-Still Self-Identification of Flux Characteristics for Synchronous Reluctance Machines Using Novel Saturation Approximating Function and Multiple Linear Regression," *IEEE Trans. Ind. Appl.*, vol. 52, no. 4, pp. 3083–3092, Jul. 2016.

[7] H. Chen, C. Sun, and Q. Wang, "Analysis of Flux-Linkage Characteristics of Switched Reluctance Linear Generator," *IEEE Trans. Appl. Supercond.*, vol. 24, no. 3, pp. 1–5, Jun. 2014.

[8] H. Chen, W. Yan, and Q. Wang, "Electromagnetic Analysis of Flux Characteristics of Double-Sided Switched Reluctance Linear Machine," *IEEE Trans. Appl. Supercond.*, vol. 26, no. 4, pp. 1–7, Jun. 2016.

[9] A. Di Gioia, I. P. Brown, Y. Nie, R. Knippel, D. C. Ludois, J. Dai, S. Hagen, and C. Alteheld, "Design and Demonstration of a Wound Field Synchronous Machine for Electric Vehicle Traction With Brushless Capacitive Field Excitation," *IEEE Trans. Ind. Appl.*, vol. 54, no. 2, pp. 1390–1403, Mar. 2018.

[10] P. Haghgooei, B. Nahid-Mobarakeh, N. Takorabet, and D. Arab-Khaburi, "Online Stator Flux Estimation for a Wound Rotor Synchronous Machine (WRSM)," in *Ind. Appl. Soc. IEEE-IAS Annu. Meet.*, pp. 1–6, Oct. 2020, iSSN: 2576-702X.

[11] P. Haghgooei, E. Jamshidpour, N. Takorabet, D. Arab-khaburi, and B. Nahid-Mobarakeh, "Magnetic Model Identification of Wound Rotor Synchronous Machine Using a Novel Flux Estimator," *IEEE Trans. on Ind. Applicat.*, pp. 1–1, 2021.

[12] K. Liu, J. Feng, S. Guo, L. Xiao, and Z.-Q. Zhu, "Identification of Flux Linkage Map of Permanent Magnet Synchronous Machines Under Uncertain Circuit Resistance and Inverter Nonlinearity," *IEEE Trans. Industr. Inform.*, vol. 14, no. 2, pp. 556–568, Feb. 2018.

[13] Y. Nie, D. C. Ludois, and I. P. Brown, "Deadbeat-Direct Torque and Flux Control of Wound Field Synchronous Machine at Low Sampling to Fundamental Frequency Ratios," *IEEE Trans. Ind. Appl.*, vol. 55, no. 4, pp. 3813–3822, Jul. 2019.

[14] M. Seilmeier and B. Piepenbreier, "Identification of steady-

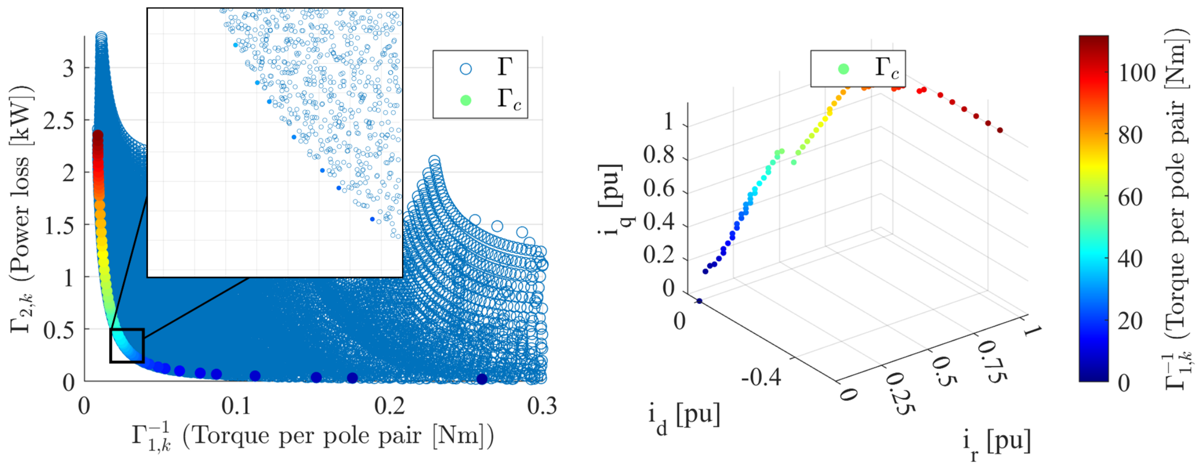


Fig. 12: Experimental results: (Left) All simulated points $\Gamma$ and convex pareto-optimal solutions $\Gamma_c$, (Right) corresponding three-dimensional MPLPT currents that will be used to construct $h(T)$

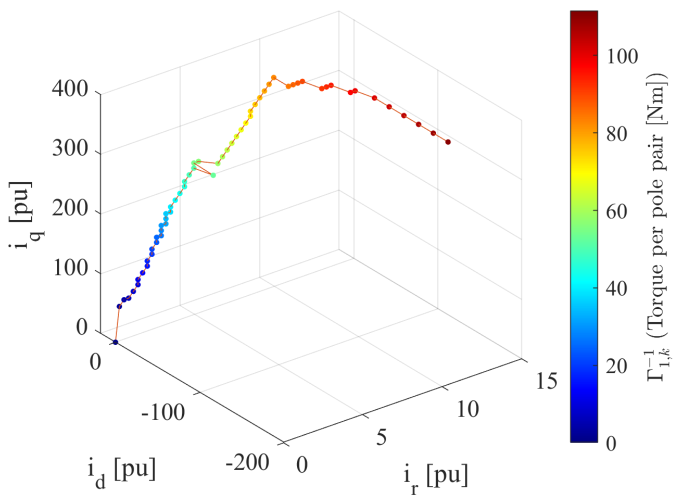


Fig. 13: MPLPT piecewise affine function $h(T)$ for simulated WRSM

state inductances of PMSM using polynomial representations of the flux surfaces," in *IECON - 39th Annu. Conf. IEEE Ind. Electron. Soc.*, pp. 2899–2904, Nov. 2013, iSSN: 1553-572X.

[15] Y. Zhang, W. Liu, Q. jia, N. Jiao, and J. Pang, "Maximum Torque per Ampere Control with Inductance and Field Current Estimation for Wound-Rotor Synchronous Starter/Generator," in *23rd Int. Conf. Electr. Mach. Syst. (ICEMS)*, pp. 172–176, Nov. 2020.

[16] Y. Kim and K. Nam, "Copper-Loss-Minimizing Field Cur-

[20] M. Preindl, "Robust control invariant sets and lyapunov-based mpc for ipm synchronous motor drives," *IEEE Transactions on Industrial Electronics*, vol. 63, DOI 10.1109/TIE.2016.2527722,

rent Control Scheme for Wound Synchronous Machines," *IEEE Trans. Power Electron*, vol. 32, no. 2, pp. 1335–1345, Feb. 2017.

[17] J. Pang, W. Liu, N. Jiao, J. Wang, and P. Ma, "Calculation of Cross-Coupling Inductance and Electromagnetic Torque in Wound-Rotor Synchronous Starter/Generator," *IEEE Trans. Ind. Electron*, vol. 66, no. 7, pp. 5115–5123, Jul. 2019.

[18] I. Canay, "Causes of discrepancies on calculation of rotor quantities and exact equivalent diagrams of the synchronous machine," vol. PAS-88, pp. 1114–1120.

[19] M. Preindl and S. Bolognani, "Optimal state reference computation with constrained mtpa criterion for pm motor drives," *IEEE Trans. Power Electron.*, vol. 30, no. 8, pp. 4524–4535, 2015.

no. 6, pp. 3925–3933, 2016.

[21] S. D. Sudhoff, *Transformer Design*, pp. 205–253, 2014.

[22] N. Kutkut, D. Novotny, D. Divan, and E. Yeow, "Analysis of winding losses in high frequency foil wound inductors," in *IAS '95. Conference Record of the 1995 IEEE Industry Applications Conference Thirtieth IAS Annual Meeting*, vol. 1, DOI 10.1109/IAS.1995.530388, pp. 859–867 vol.1, 1995.

[23] M. Eull, L. Zhou, M. Jahnes, and M. Preindl, "Bidirectional nonisolated fast charger integrated in the electric vehicle traction drivetrain," *IEEE Transactions on Transportation Electrification*, vol. 8, DOI 10.1109/TTE.2021.3124936, no. 1, pp. 180–195, 2022.

[24] V. Pareto, *Manual of political economy (manuale di economia politica)*. New York: Kelley, 1971 (1906), translated by Ann S. Schwier and Alfred N. Page.

[25] L. He, A. Friedman, and C. Bailey-Kellogg, "A divide-and-conquer approach to determine the pareto frontier for optimization of protein engineering experiments," *Proteins*, vol. 80, DOI 10.1002/prot.23237, pp. 790–806, 03 2012.

[26] P. Samuel and S. Levy, *Projective Geometry*, ser. Undergraduate Texts in Mathematics. Springer New York, 1988.

[27] F. Borrelli, A. Bemporad, and M. Morari, "Predictive control for linear and hybrid systems," 2017.